



## Seismic Resistance of Breakwater Foundation Reinforced by Steel Sheet Pile and Gabion - Evaluation through Element Test -

T. Hara<sup>(1)</sup>, H. Hazarika<sup>(2)</sup>, B. Chaudhary<sup>(3)</sup>, N Yamasaki<sup>(4)</sup>, K. Nishimura<sup>(5)</sup>

<sup>(1)</sup> Professor, Kochi University, haratd@kochi-u.ac.jp

<sup>(2)</sup> Professor, Kyushu University, hazarika@civil.kyushu-u.ac.jp

<sup>(3)</sup> Ph.D. student, Kyushu University, babloomit@gmail.com

<sup>(4)</sup> Engineer, Yonden Consultants Inc., n-yamasaki@yon-c.co.jp

<sup>(5)</sup> Graduate student, Kyushu University, kazenotani.no.tarao@gmail.com

...

### Abstract

Many coastal protection facilities were damaged by the 2011 Off the Pacific Coast of Tohoku Earthquake and the subsequent tsunami, which spread inundation to the coastal plain area. Countermeasures of compound disaster by future mega earthquake such as, Nankai trough earthquake having high probability etc., are issues that should be resolved urgently. The resilient structures that can reduce damage when they are subjected to earthquake and tsunami higher than the design earthquake and tsunami are being developed. A resilient reinforcement technique of breakwater foundation using gabion mound (mound covered with gabion) and steel sheet pile that can minimize damage when the tsunami is higher than the design tsunami height has been developed by Hazarika, et al. (2015). Model tests for evaluating the technique using 1G shaking table has been described in a series paper by Hazarika et al. (2017).

In this paper, elements tests were performed for the materials used in foundation materials of the 1G model shaking table test to evaluate the material behavior under cyclic loading. The authors performed monotonic and cyclic triaxial tests for the rubble used as mound material in the model test to evaluate shear deformation properties during static and dynamic loading. Results of this research show that the mound material can mobilize excellent shear resistance under both static and seismic loading condition. The undrained shear strength of the crushed stone used for foundation materials showed a value larger than the gravelly soil and sand of the equal relative density. The cyclic undrained shear strength of the crushed stone showed cyclic mobility during shearing, and also excess pore water pressure ratio  $\Delta u/\sigma'_c$  did not reach the perfection liquefaction state defined in 0.95. From the triaxial test results, crushed stone used for mound material was found to have a very large shear resistance. Therefore, it can be inferred that the material contributes to the stability of caisson at all times including under seismic loading.

*Keywords: Breakwater, Triaxial test, undrained shear strength*



## 1. Introduction

The 2011 Great East Japan Earthquake resulted in powerful shocks and induced a tsunami that extensively damaged coastal protection facilities, such as breakwaters and seawalls. Japan's Sanriku region has repeatedly experienced large tsunamis in the past, and therefore had engaged in various measures to mitigate damage, such as the construction of breakwaters and seawalls, architectural fortification of residential structures, and relocation to higher ground. However, the tsunami resulting from the Great East Japan Earthquake caused flooding to previously unimagined heights, leading to extensive damage to coastal protection facilities and thus to widespread flooding within areas though to be protected. The Japanese Ministry of Land, Infrastructure, Transport and Tourism [1, 2] classifies patterns of damage to breakwaters due to the Great East Japan Earthquake into "overflow scour type", "tsunami wave-force type", "bank-head scour type", and "drawback water-level-difference type". We examine these disaster patterns with the primary aim of revealing vulnerabilities in breakwater foundation mounds. This should assist in improving earthquake- and tsunami-resistant designs.

There have been many studies and investigations related to coastal protection facilities, such as breakwaters and seawalls that experienced damage due to the Great East Japan Earthquake [3, 4]. Using disaster assessment focused on coastal plains areas, Hara et al. [5, 6] provided an overview of the scour damage seen in coastal protection facilities.

This study is a part of the undergoing research for mitigating damage to breakwaters when that damage results from a combination of earthquake and tsunami damage. These measures include building breakwater foundations with sheet pilings and a gabion-type mound (in which a rubble mound is completely surrounded by a gabion) or gabion facing (in which gabions are used for mound facings). Such techniques are expected to minimize damage through improved anti-earthquake features and to increase toughness even in the face of large tsunamis that exceed designed heights [7]. Fig.1 shows an overview of the reinforcement structures.

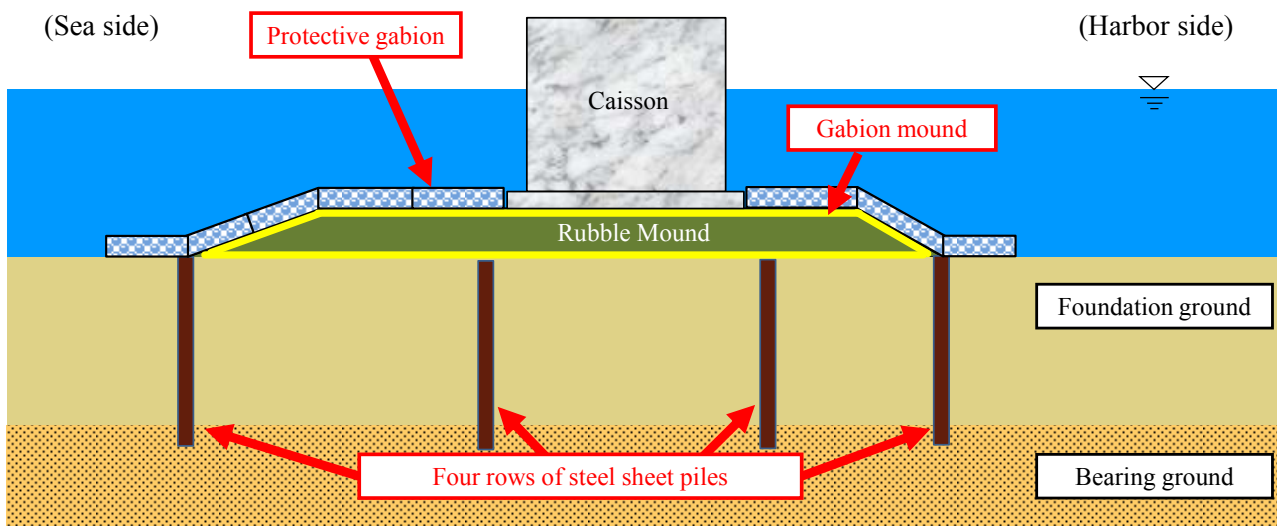


Fig.1 - Reinforcement technique for improved breakwater toughness (from Hazarika et al. [7])

In previous studies, Hara et al. [8, 9, 10] performed systematic experiments involving laboratory triaxial tests to investigate the mechanical properties of materials used in caisson-type breakwaters, and evaluated shear characteristics at monotonic loading and during earthquakes through comparison of conglomerate materials and sandy soils with various particulate forms. Monji et al. [11] and Hazarika et al. [12] performed vibration table experiments in a 1G gravitational field to demonstrate that sheet pilings suppress lateral flow in the foundation ground directly beneath the breakwater, thereby creating a subsidence suppression effect on the caisson and



mound, and that the restraint effect of gabion reinforcement suppresses subsidence, tilting, and horizontal displacement of the caisson.

Model tests for evaluating the technique using 1G shaking table has been described in a different paper in this series by Hazarika et al. [13]. With the goal of elucidating the structural and dynamic features of basic mound materials as well as their combined effects, we performed element tests in this research. We performed laboratory triaxial tests as element tests to understand the shear characteristics of breakwater foundations during earthquakes. To evaluate the shear characteristics of mound materials used in caisson-type breakwaters at monotonic loading and during earthquakes, we performed laboratory triaxial tests on materials of varying granularity and particle shape, comparing the results to those from tests on samples with the same relative density. This allows investigating the static and dynamic features of mound materials.

## 2. Mound material shear characteristics from triaxial testing

To evaluate the shear characteristics of mound materials (crushed stone) at monotonic loading and during earthquakes, we performed consolidated undrained triaxial testing and cyclic undrained triaxial testing

### 2.1 Test material overview

Fig.2 shows the grain size distribution curve for the material used in the experiments, and Table 1 lists its physical properties. Sample A is No. 6 crushed stone taken from the Kyushu region; it is a gravelly soil with uniformity coefficient  $U_c$  of 1.5 that features hard, strongly angled particles. Sample B is a gravelly soil of riverbed sediment taken through disturbed collection from the estuary of the Niyodo River in Kochi Prefecture, laboratory treated to have the same particle size composition as Sample A. While this soil, too, has hard particles, they are more rounded than those found in Sample A. Sample C is a sandy gravel with good particle size distribution  $U_c$  of 11.4, prepared to have a maximum particle diameter  $D_{max}$  of 19mm. Sample D is a sandy soil taken from a levee foundation in the Yoshihama district of Iwate Prefecture, prepared to have the same granularity distribution as Toyoura sand (Sample E); it contains a large amount of weathered granite soil (Masa soil).

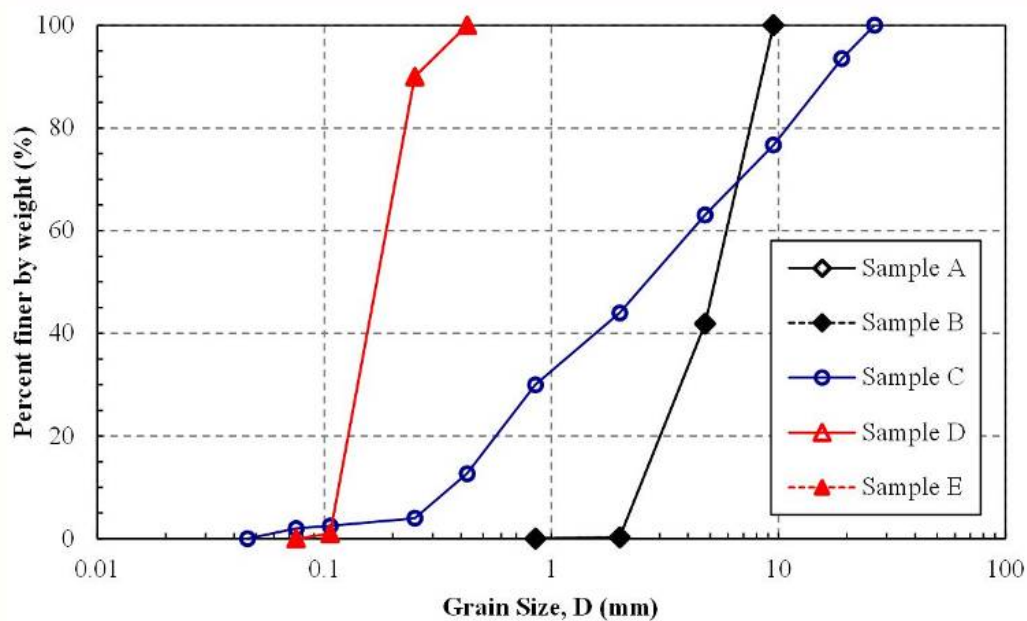


Fig.2 - Grain size distribution curves for the material used in the experiments



Table 1 - Physical property for the material used in the experiments

Materials	$\rho_s$ (g/cm <sup>3</sup> )	$\rho_d$ (g/cm <sup>3</sup> )	$\rho_{dmax}$ (g/cm <sup>3</sup> )	$\rho_{dmin}$ (g/cm <sup>3</sup> )	$U_c$	$U_c'$	$D_{50}$ (mm)	$I_P$
Sample A (Crushed stone)	2.773	1.620	1.781	1.416	1.5	1.4	4.7	NP
Sample B (Gravelly soil)	2.731	1.720	1.844	1.535	1.5	1.4	4.7	NP
Sample C (Sand gracel)	2.727	1.980	2.143	1.768	11.4	0.5	2.7	NP
Sample D (Masa soil)	2.700	1.132	1.256	0.987	1.7	3.8	0.16	NP
Sample E (Toyoura sand)	2.640	1.506	1.639	1.336	1.7	3.8	0.16	NP

## 2.2 Test methods

We performed consolidated undrained triaxial compression testing and cyclic undrained triaxial testing. The soil specimen can be cyclically loaded from above as a stress-control test and monotonically loaded from below as a strain-control test as indicated in Fig.3. Specimens for triaxial testing were of the middle size (diameter 100 mm and height 200 mm) for Samples A, B, and C, while Samples D and E were of the small size (diameter 50 mm and height 100 mm).

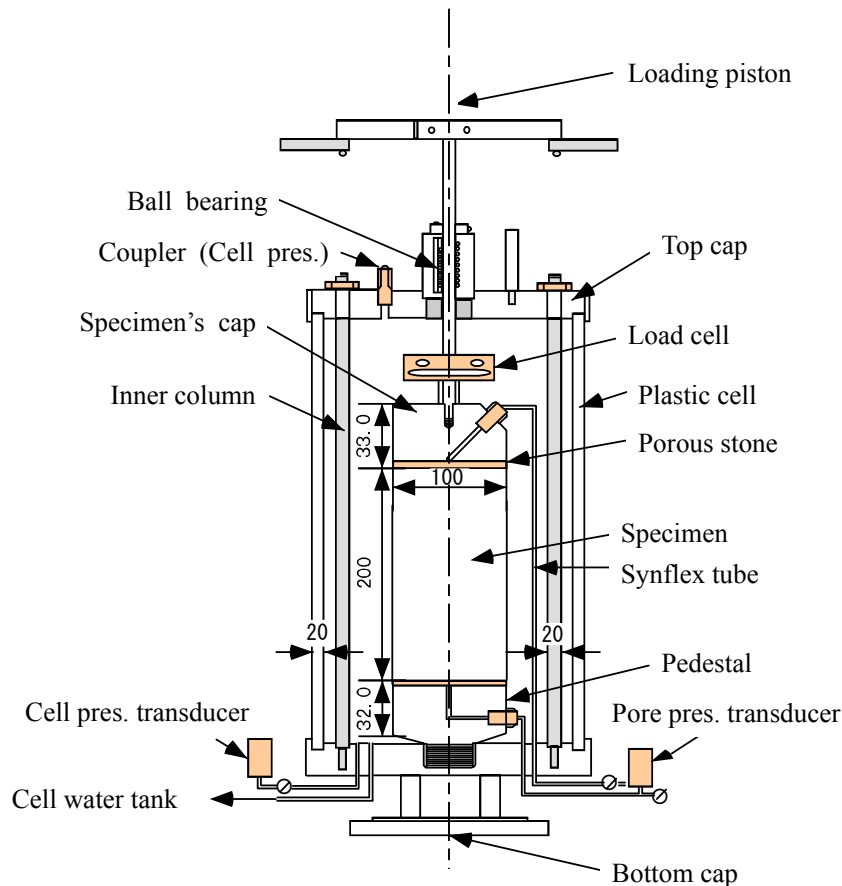


Fig.3 - Triaxial test apparatus used in this research (Examples of diameter 100mm specimen)



Specimen preparation was performed as follows, adopting varying methods according to features of the specimen. For Sample A, in consideration of breakwater rubble mounds used in previous model experiments, we set dry density following compression  $\rho_d$  as  $1.620 \text{ g/cm}^3$ , employing the wet tamping method to simulate actual mound construction methods. The specimen was divided into five layers, with each mold compressed by using a rubber hammer. The relative specimen relative density  $D_r$ , as calculated from minimum and maximum gravel density testing, was 60%. The dry densities of Samples B–E were set to the same relative density as Sample A ( $D_r = 60\%$ ), according to values for minimum and maximum dry density as calculated from minimum and maximum gavel density testing. Samples B, D, and E were created using the wet placement vibration method, whereas the material for Sample C was created using the wet tamping method to prevent material sorting. Surface roughness was low for all specimens, so membrane penetration correction was not performed.

Each specimen was saturated through CO<sub>2</sub> compression, applying backpressure of 98 kPa until a pore pressure coefficient  $B$  of 0.96 was confirmed. Consolidated undrained triaxial compression testing for each specimen was conducted on isotropically consolidated specimens at consolidation stress  $\sigma'_c = 98 \text{ kPa}$  and strain rate  $0.1\%/min$ . Monotonic loading in the undrained condition was conducted until axial strain  $\varepsilon_a$  of the specimen reached 15%. In consideration of actual breakwater mound facings, consolidation stress for Sample A was applied in three stages ( $\sigma'_c = 49, 98, 196 \text{ kPa}$ ). For purposes of comparison, monotonic loading under the same conditions was applied to Sample E. To further investigate the effects of particle fragmentation under low axial strain, we also performed experiments after stopping loading as soon as an axial strain of 1% was reached. Cyclic undrained triaxial testing was performed through repeated application of a 0.1 Hz sine wave load under the undrained conditions after isotropic consolidation at consolidation pressure  $\sigma'_c = 98 \text{ kPa}$ , with repeated load applied until double amplitude axial strain  $DA$  reached 10%.

### 3. Triaxial tests results

#### 3.1 Consolidated undrained triaxial compression testing

Fig.4 shows the relation between main stress difference and axial strain for each material, with specimens in triaxial compression testing at consolidation pressure  $\sigma'_c = 98 \text{ kPa}$ . Comparing specimens in terms of the relation between main stress difference and axial strain, increased axial strain uniformly increases main stress difference for Samples A, B, and C, with no clear peak in maximum main stress difference seen up to an axial strain  $\varepsilon_a$  range of 15%. In comparison, the uniformity coefficient for Sample C ( $U_c = 11.4$ ) is largely different from those of Samples A and B ( $U_c = 1.5$ ), though it is interesting to note the similar trend in change of the main stress difference due to increased axial strain. Unlike materials containing gravel, Sample E shows a peak main stress difference at relatively small ranges of axial strain, in the area of  $\varepsilon_a = 5\%$ , and thereafter shows a constant value. As it does in Sample A, the strain level of Sample D increases at ranges of axial strain  $\varepsilon_a$  below 1%; however, following that, the increase of main stress difference with regard to axial strain becomes smaller. When comparing the relation between excess pore pressure and axial strain, Samples A and B generate negative pressure immediately after the start of compression, demonstrating a high material characteristic for shear behavior. Sample C generates positive excess pore pressure immediately after the start of loading, but although negative excess pore pressure well coincides with increased axial strain, a high material characteristic for shear behavior is demonstrated. Samples D and E show a similar tendency for excess pore pressure to asymptotically approach a constant value at an early stage after the start of loading, but Sample D has a notable positive excess pore pressure, and that of Sample E is negative. In other words, even for materials having similar relative densities and uniformity coefficients, there are large differences in the manner of variation of excess pore pressure accompanying increases in axial strain.

Fig.5 shows the effective stress path for Sample A (crushed stone). The relation between mean effective main stress  $p'$  and deviatoric stress  $q$  shows a nearly monotonic increase until the failure envelope is reached. The limit state index  $M_f$  is calculated as 1.850, and the angle of internal friction angle  $\phi'$  is  $45^\circ$ . In contrast, the limit state index  $M_f$  for Sample E (Toyoura sand) is calculated from consolidated undrained triaxial testing as 1.068, and the angle of internal friction angle  $\phi'$  is  $27^\circ$ . In other words, crushed stone has a very large angle of shearing resistance as compared with Toyoura sand of the same relative density.

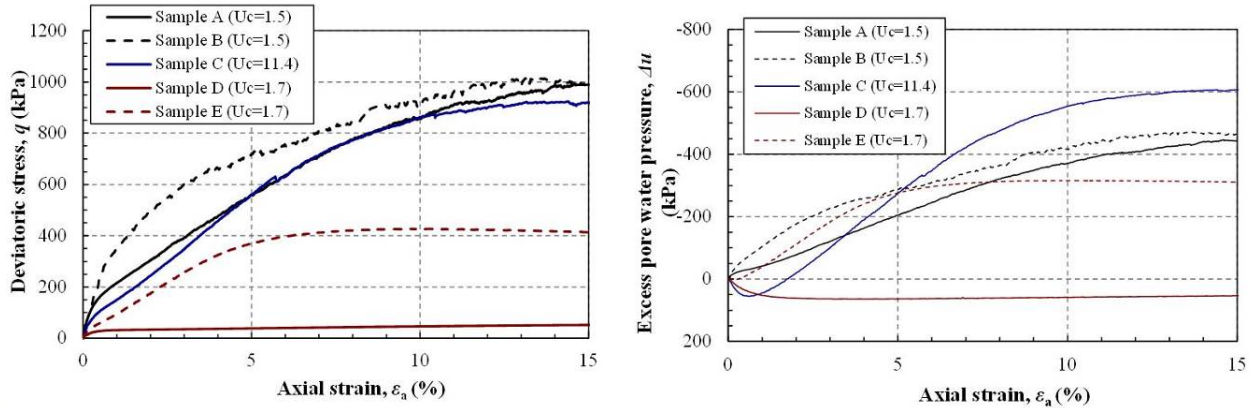


Fig.4 - Relationship between main stress difference and axial strain

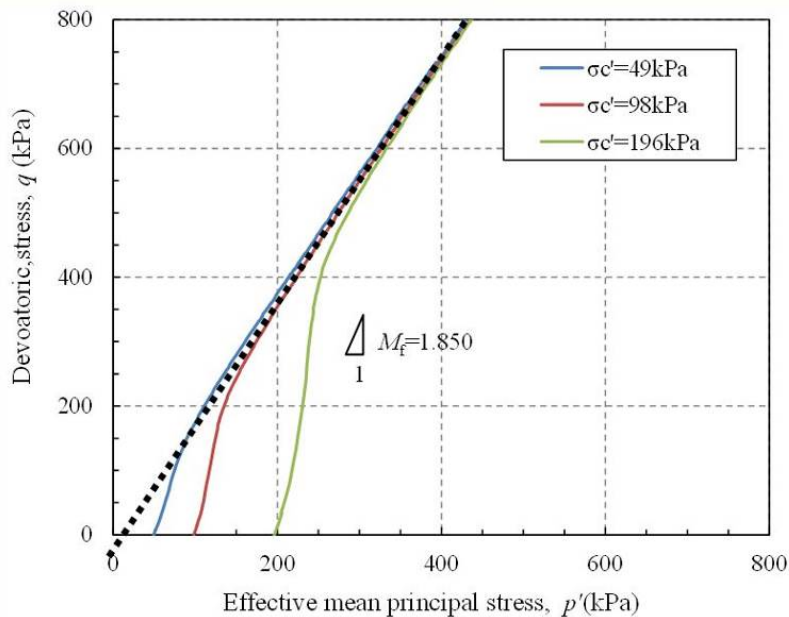


Fig.5 - Effective stress path for Sample A

Fig.6 summarizes the effective stress path for each sample at consolidation pressure  $\sigma'_c = 98$  kPa. Overall, there is remarkable deviatoric stress in materials with larger mean particle diameter  $D_{50}$ , demonstrating an upward-developing stress path. Samples A and B, which have a small and equal uniformity coefficient for the particle size distribution ( $U_c = 1.7$ ,  $D_{50} = 4.7$ ), have a similar trajectory despite their different particle shapes, but similar trajectories are not seen for Samples D and E, despite their equal uniformity coefficient for particle size ( $U_c = 1.7$ ,  $D_{50} = 0.16$ ). This means that it is more difficult for the deviatoric stress  $q$  of Sample D to increase than for the deviatoric stress of Sample E to do so, which is because of Samples D's prominent particle fragmentation accompanying increased axial strain. Sample C ( $U_c = 11.4$ ,  $D_{50} = 2.7$ ) has hard particles, and because it contains a large amount of sand content well distributed as a matrix, positive excess pore pressure occurs at initial shear, and mean effective main stress  $p'$  decreases, but recovers when negative dilatancy is prominent. This series of experimental results shows that materials with hard particles have small uniformity coefficients, and larger mean



particle diameters are associated with larger shear resistance forces. In sandy soils having the same granularity distributions, differences in friability result in large differences in the stress path.

Fig.7 compares granularity distributions before and after loading for each material. Despite Sample A having hard particles, after shear testing the particle size composition shifts toward that of sandy soils. Sample D is Masa soil formed from soft and weak weathered soil in which the granularity distribution largely changes after shear, but it is interesting that it has a trend similar to that of Sample A despite the differences in soil particle hardness. Because Samples B, C, and E are materials with hard soil particles, there is only minor change in post-shear particle size composition.

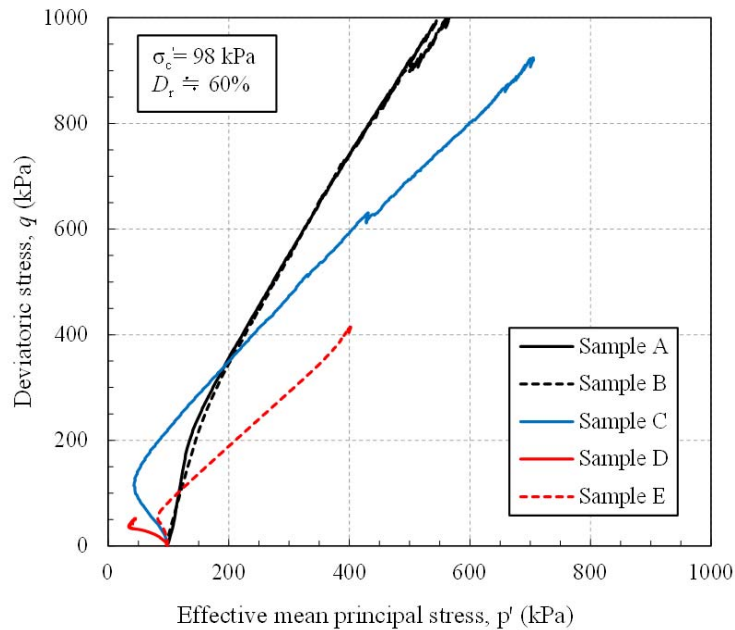


Fig. 6 - Effective stress path for each sample ( $\sigma'_c = 98$  kPa)

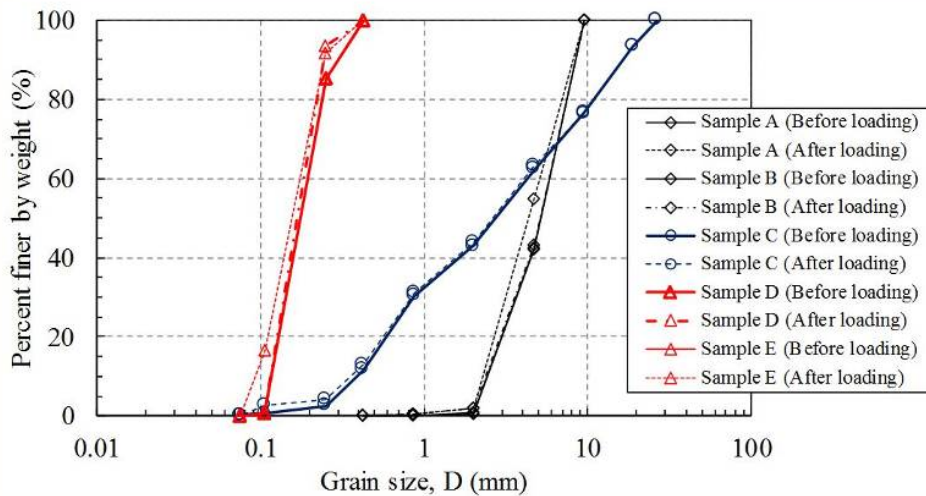


Fig.7 - Grain size distribution curves after monotonic loading tests



Fig.8 shows the particle breakage rate  $B_M$  for each material, as calculated from the particle size distributions before and after the load test shown in Fig.7. Table 2 summarizes the ratio  $B_{M1} / B_{M15}$  between the particle breakage rate  $B_{M15}$  at the point where axial strain  $\epsilon_a = 15\%$  and the rate  $B_{M1}$ , where  $\epsilon_a = 1\%$ . The particle breakage rate is calculated following the method of Marsal [14], finding the breakage rate when loading is stopped immediately after axial strain  $\epsilon_a$  reaches the prescribed value (1% or 15%). Samples B and C, which are prepared from riverbed gravel with hardness before and after load testing, show almost no particle fragmentation even after compression to  $\epsilon_a = 15\%$ . Sample E (Toyoura sand) has hard soil particles, but shows particle fragmentation to a small extent. This is in agreement with the results of previous research by Hara et al. [15]. Overall, Samples B, C, and E do not show much particle fragmentation. The  $B_{M1} / B_{M15}$  ratio is similar, at around 6-7%, and particle fragmentation at initial load does not rapidly occur. In contrast, Samples A (crushed stone) and D (Masado soil) have different soil particle hardnesses, yet particle fragmentation still occurs even when axial strain remains small. The  $B_{M1} / B_{M15}$  ratio is thus much higher in comparison with that of sand and sand gravel with hard soil particles.

From the above discussion of particle fragmentation, we find that materials with hard soil particles express high shear strength regardless of difference in particle form, and that the crushed stone used in caisson foundations expresses extremely high shear strength even in the case of approximately 1% strain. We determine that while crushed stone holds the potential for particle fragmentation in the consolidation and shearing process, it has the shear strength of rounded gravel materials of the same relative density, uniformity coefficient, and mean particle diameter.

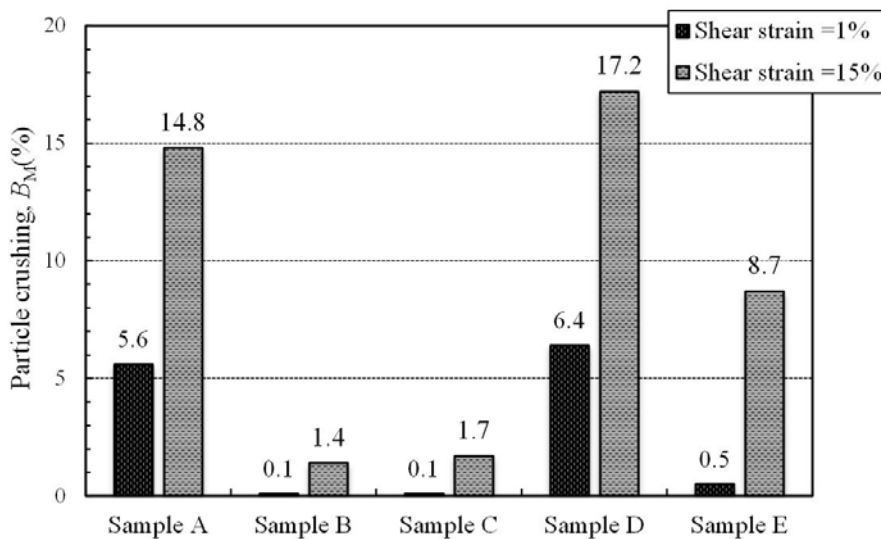


Fig 8 - Comparison of the particle breakage ratio

Table 2 - Proportion of particle breakage ratio

	Sample A	Sample B	Sample C	Sample D	Sample E
$\epsilon_a = 1\%, B_{M1}$ (%)	5.6	0.1	0.1	6.4	0.5
$\epsilon_a = 15\%, B_{M15}$ (%)	14.8	1.4	1.7	17.2	8.7
$B_{M1}/B_{M15} \times 100$ (%)	38	7.1	5.8	37	5.7



### 3.2 Cyclic undrained triaxial testing

Fig.9-12 shows the effective stress path and the relation between axial stress difference and axial strain for Samples A, B, C, and E, respectively. The gravel materials with  $U_c = 1.5$ , shown in Figs.9 and 10 (Samples A and B), are similar in many respects. In other words, we can observe a negative excess pore pressure resulting from each application of compressive load and material features of positive dilatancy. Furthermore, even at the point where double amplitude axial strain  $DA$  reached 10% with repeated load, remarkable cyclic mobility was seen, with excess pore pressure ratio  $\Delta u/\sigma'_c$  not reaching 0.95. In contrast, Samples C and E (Figs.11 and 12, respectively) show very different effective stress paths from the gravel material with  $U_c = 1.5$ . There is an accumulation of negative axial strain (tensile direction) accompanying a decrease in mean effective principal stress  $p'$ , and fragmentation results when  $DA = 10\%$ . In comparison with the gravel material with  $U_c = 11.4$  (Fig. 12), even when relative density is the same there is a large change in excess pore pressure accompanying increases in the number of load repetitions. We infer that this difference in repeated shearing behavior is due to the existence of matrix material in the pores between soil particles. From the above, and from the facts that crushed stone does not show positive axial strain even when receiving repeated undrained shearing and that full liquefaction (defined as remarkable cyclic mobility with  $\Delta u/\sigma'_c$  of 0.95) does not occur, crushed stone has the potential to maintain breakwater stability with little shearing deformation due to repeated shearing from earthquakes.

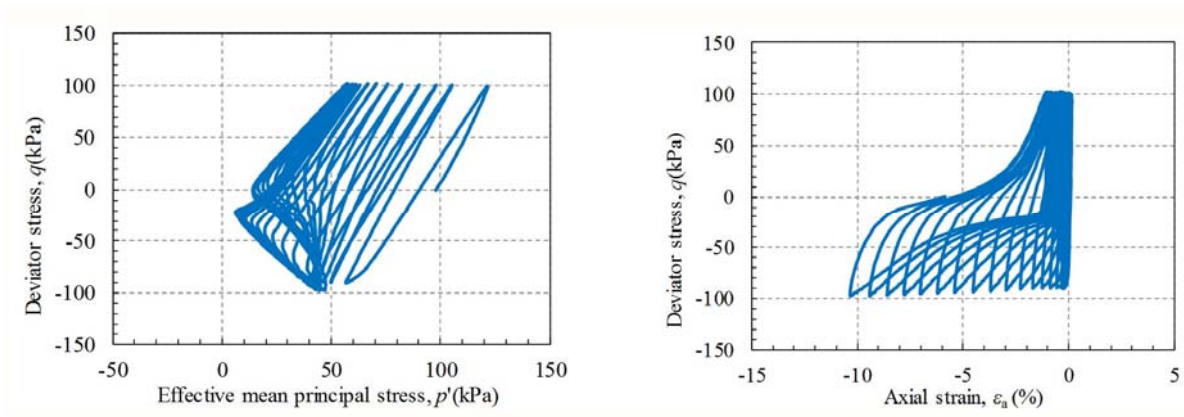


Fig.9 - Effective stress path and the relation between axial stress difference and axial strain (Sample A)

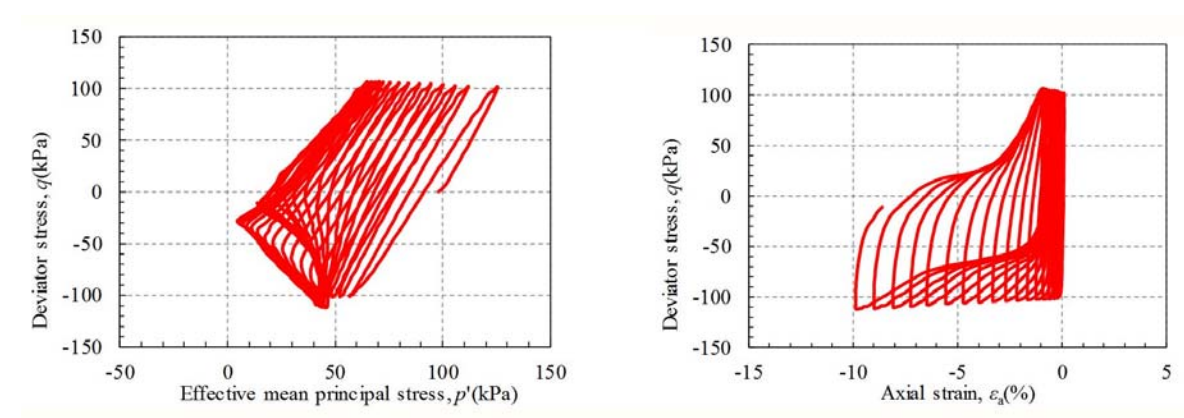


Fig.10 - Effective stress path and the relation between axial stress difference and axial strain (Sample B)

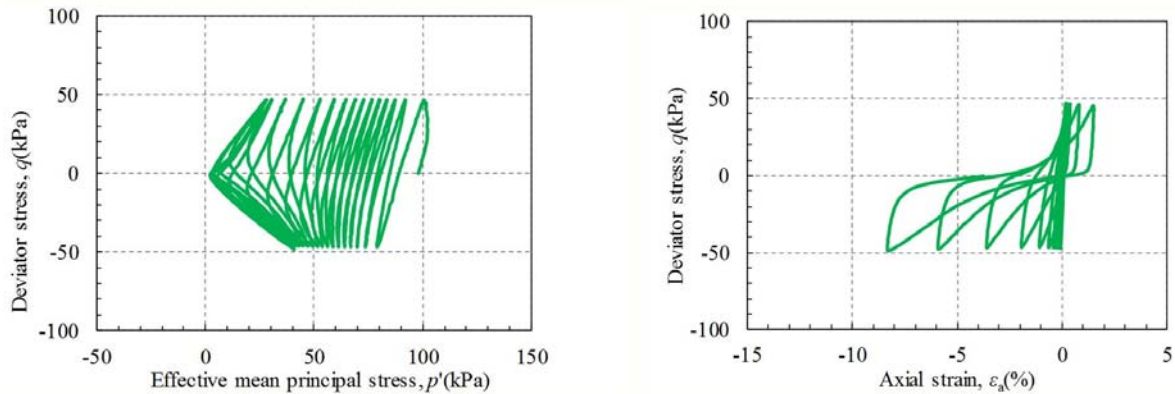


Fig.11 - Effective stress path and the relation between axial stress difference and axial strain (Sample C)

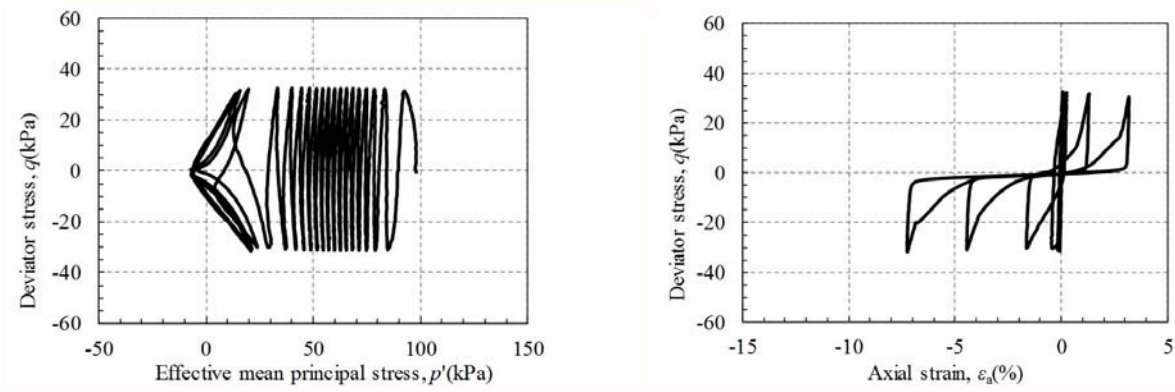


Fig.12 - Effective stress path and the relation between axial stress difference and axial strain (Sample E)

Fig.13 shows the results of cyclic undrained triaxial testing for each material as the relation between number of load repetitions  $N_c$  and the cyclic stress ratio, CSR ( $\sigma_d/2\sigma'_c$ ;  $\sigma_d$  = single axial stress amplitude and  $\sigma'_c$  = effective confining stress), when  $DA$  reached 5%. Taking the liquefaction strength  $R_{L20}$  as characterized by the repeated stress amplitude ratio at  $N_c = 20$ , the following things are seen. Samples A and B (gravel materials with small  $U_c$ ), both have higher  $R_{L20}$  than Sample E (Toyoura sand) and the large  $U_c$ -valued Sample C. The  $R_{L20}$  for Sample A was 0.42, which exceeds the levels for both Toyoura Sand ( $R_{L20} = 0.15$ ) and Sample C ( $R_{L20} = 0.18$ ).

Sample C, which has a large uniformity coefficient, has a small CSR value despite containing gravel, which we attribute to the interstitial fine fraction. Gravel materials with small uniformity coefficient did not show CSR values exceeding 0.3 for all numbers of load repetitions  $N_c$ , but did show large repeated shearing features. However, while Sample A shows large increases in CSR accompanying increases in  $N_c$  at small numbers of load repetitions, Sample B showed less such variation in CSR due to changes in  $N_c$ , despite having the same  $U_c$  values. This shows that poorly mixed gravel materials with high angularity exhibit high shear resistance with a low number of load repetitions ( $N_c$  of 10 or less), and that variations in CSR accompanying increased  $N_c$  depend on particle form.

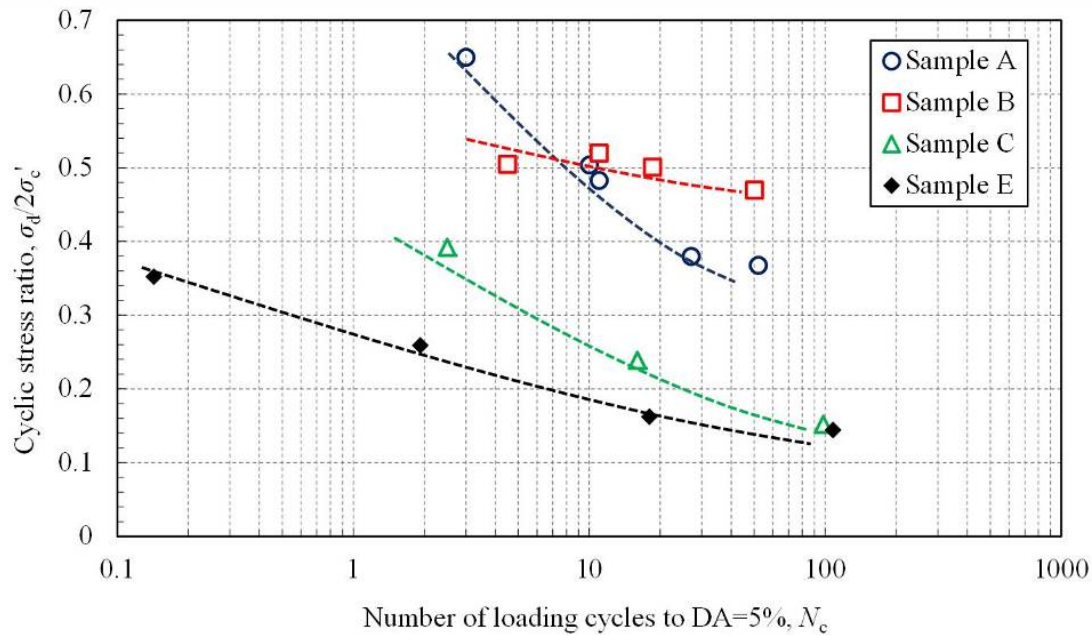


Fig.13 - Relation between number of load repetitions  $N_c$  and the cyclic stress ratio

#### 4. Conclusions

To develop breakwater structures with improved anti-earthquake designs that can withstand the external force of tsunamis, even when the tsunami height exceeds design specifications, we performed laboratory triaxial tests on materials of varying granularity and particle shape. The main findings of this study are as follows.

- 1) The consolidated undrained shear characteristics of crushed rock like that used in mound materials has large values as compared even with well-mixed rounded gravel and sandy soil with approximately same relative densities. For maximum main stress differential  $q_{max}$ , soil particle hardness is dominant over particle friability.
- 2) Crushed rock with angularity has high shear resistance with a small number (10 or fewer) of load repetitions  $N_c$ , as compared with rounded gravel and Toyoura sand having the same uniformity coefficient  $U_c$ .
- 3) Even for specimens with the same relative density after consolidation, the dynamic properties of gravel materials varied widely with differences in particle size distribution and particle form.
- 4) Even in cases where mound materials were subjected to repeated undrained shearing, there was remarkable cyclic mobility, and full liquefaction (defined as remarkable cyclic mobility with  $\Delta u/\sigma'_c$  of 0.95) did not occur.
- 5) From the fact that the crushed stone used for mound material has extremely high shearing resistance, we infer that it contributes to caisson stability at monotonic loading and during earthquakes.

#### Acknowledgements

This work was supported by a grant for priority research themes from the Japan Iron and Steel Federation, to whom we express our thanks. We also thank Akihiko Hatayama (Kochi University Geotechnical Engineering Lab, currently with Kiso-jiban Consultants Co., Ltd.), and Akiko Sakabe (Kochi University Geotechnical Engineering Lab, currently with Eight-Japan Engineering Consultants, Inc.) for their extensive support on technical aspects of this research.



## References

- [1] MLIT (2011): Earthquake and tsunami resistant measures against ports in Tohoku area. *Technical Committee Report No. 3. Ministry of Land, Infrastructure, Transport and Tourism, Government of Japan.* (in Japanese)
- [2] MLIT (2013): Guidelines for earthquake resistant design of breakwaters. *Reference Materials. Ministry of Land, Infrastructure, Transport and Tourism, Government of Japan.* (in Japanese)
- [3] Hazarika, H., Hara, T., and Furuichi, H. (2013): Soil structure interaction during earthquake and tsunami- Two case studies from the latest disaster in Japan. *Proc. of the 18<sup>th</sup> International Conference on Soil Mechanics and Geotechnical Engineering*, Paris, France, 131-142.
- [4] Hazarika, H., Kasama, K., Suetsugu, D., Kataoka, S., and Yasufuku, N. (2013): Damage to geotechnical structures in waterfront areas of northern Tohoku due to the march 11, 2011 tsunami disaster. *Indian Geotechnical Journal*, 43(2), 137-152.
- [5] Hara, T., Ohkawara, M., Ohsumi, T., Yamanaka, M., Ishihara, Y. and Tsunekawa, Y. (2012): Damage of southern central part of coastal region of Iwate prefecture due to Off the Pacific Coast of Tohoku Earthquake. *Japan Geotechnical Journal*, 7(1), 25-36. (in Japanese)
- [6] Hara, T., Okamura, M., Uzuoka, R., Ishihara, Y. and Ueno, K. (2012): Damages to River Dikes Due to Tsunami in South-central Coastal Area of Iwate Prefecture. *Japan Geotechnical Journal*, 7(1), 253-264. (in Japanese)
- [7] Hazarika, H., Hara, T., Nishimura, K., Yamasaki, N., Monji, N., Chaudhary, B., Ishikura, R., and Kasama, K. (2015): Fundamental Study on Seismic Resistant Behavior of Caisson Type Breakwater Foundation Reinforced by Steel Sheet Pile and Gabion. *Journal of Japan Association for Earthquake Engineering*, 16(1), 184-204. (in Japanese)
- [8] Hara, T., Yamasaki, N., Hatayama, A. and Sakabe, A. (2013): Examination on the shear properties of the caisson breakwater mound. *Proc. of Japanese Geotechnical Society Shikoku Branch Annual Meeting*, 39-40. (in Japanese)
- [9] Hara, T., Yamasaki, N., Hatayama, A., Hazarika, H. and Monji, N. (2014): Study on the dynamic characteristics of the Caisson breakwater mound material. *Proc. of the 49<sup>th</sup> Japanese Geotechnical Society Annual Meeting*, 1485-1486. (in Japanese)
- [10] Hara, T., Yamasaki, N., Hazarika, H. and Monji, N. (2014): Fundamental experiments on the shear properties of backwater mound materials. *Proc. of Japanese Geotechnical Society Shikoku Branch Annual Meeting*, 13-14. (in Japanese)
- [11] Monji, N., Hazarika, H., Ishikura, R., Kasugai, Y., Kasama, K., Hara, T., and Yamazaki, N. (2014): Experimental verification on earthquake resistance of a new reinforcement technique for breakwater using steel sheet pile and gabion. *Proc. of the Japanese Geotechnical Society Special Symposium on the Great East Japan Earthquake*, Tokyo, 724-730. (in Japanese)
- [12] Hazarika, H., Hara, T., Monji, N., Yamazaki, N., Nishimura, K., Ishikura, R., and Kasama, K. (2014): Experimental study on earthquake resistance reinforcing method of breakwater foundation. *Proc. of the 59<sup>th</sup> Geotechnical Engineering Symposium*, Nagano, 443-450. (in Japanese)
- [13] Hazarika, H., Hara, T., Chaudhary, B., Nishimura, K., Yamasaki, N., and Kasama, K. (2017): Seismic Resistance of Breakwater Foundation Reinforced by Steel Sheet Pile and Gabion - Evaluation through Model Shaking Table Test -. *Proc. of the 16<sup>th</sup> World Conference on Earthquake Engineering (16<sup>th</sup> WCEE)*, Paper no. 707.
- [14] Marsal, R.J. (1972): Mechanical properties of rockfill. *Casagrande Volume*, Joho Wiley & Sons, 109-200.
- [15] Hara, T., Ueno, M., Nakase, H., Hayashi, K. (2011): Relationship between shear strength of sandy soil with different particle strength and particle breakage volume. *Proc. of the 46<sup>th</sup> Japanese Geotechnical Society Annual Meeting*, 361-362. (in Japanese)